Available online at www.sciencedirect.com

SciVerse ScienceDirect

Ceramics International 39 (2013) 5751–5763

CERAMICS INTERNATIONAL

www.elsevier.com/locate/ceramint

Effect of milling parameters on the formation of nanocrystalline hydroxyapatite using different raw materials

Bahman Nasiri-Tabrizi*, Abbas Fahami, Reza Ebrahimi-Kahrizsangi

Materials Engineering Department, Najafabad Branch, Islamic Azad University, Najafabad, Isfahan, Iran

Received 9 December 2012; received in revised form 12 December 2012; accepted 30 December 2012
Available online 9 January 2013

Abstract

The influence of milling parameters (time and atmosphere) on the mechanochemical synthesis of nanocrystalline hydroxyapatite (n-HAp) using different raw materials was studied. Two distinct chemical reactions were activated for various milling times under air or in a high purity argon (99.998 vol%) atmosphere. Then, the mechanically activated powder was heat treated at 800 °C for 1 h to produce n-HAp with high degree of crystallinity. Results revealed that the phase purity of products under both milling atmospheres was strongly influenced by the chemical composition of raw materials. The synthesized powders exhibited average sizes about 32 and 27 nm under air atmosphere, and about 32 and 34 nm under argon atmosphere. The fraction of crystalline phase drastically decreased after 80 h of milling under both atmospheres. In addition, the fraction of crystalline phase for the annealed sample at 800 °C was higher than the mechanosynthesized specimens. The results of morphological evaluation confirmed the formation of n-HAp with different morphologies each of which can be used for particular purpose.

Keywords: Nanocrystalline hydroxyapatite; Milling atmosphere; Mechanochemical; Annealing

1. Introduction

Hydroxyapatite (HAp, $Ca_{10}(PO_4)_6(OH)_2$), as the major mineral constituents of vertebrate bone and tooth, is the most well-known bioceramic from the apatitic family. Generally, HAp is used in the coating of metallic implants, repairing of bone defects and bone augmentation due to its superior biocompatibility, osteoconductivity and bioactivity [1]. In addition, HAp and its substituted structures have also been served for drug delivery [2], gene therapy [3], chromatography [4] and waste water remediation [5]. Depending on the application, there is often a need for the nanoparticles to be in a particular size range [6]. Nanocrystalline HAp (n-HAp) with higher surface area and lower particle size can provide higher biocompatibility, greater catalytic activity and good adsorption capability for use as biomaterial, catalyst and adsorbent [7]. Therefore, many investigations have been carried out to synthesize n-HAp [8–11]. Nanocrystalline HAp with desired properties can be achieved by control of the product characteristics such as particle size and shape, particle distribution and agglomeration [12].

There are several sources for the treatment of bone diseases that have been faced with restrictions [13]. Consequently, research on production of calcium phosphates is likely to continue until suitable and cost-effective methods to be found. The obtained HAp from varied powder processing routes has great potential for bone substitute due to its excellent osteoconductive properties [14]. It has been found that the n-HAp can bond directly to tissues and promotes tissue growth and thus it has been considered in orthopedic and dental applications [15]. Generally, the fabrication methods of the n-HAp can be classified into two groups: wet and dry [16]. In wet process, the by-product is almost water as a result the probability of contamination during the process is very low. On the other hand, the dry process has benefit of high reproducibility and low processing cost [17,18]. Among different dry processes, mechanochemical treatment has recently been receiving particular attention as an alternative method to prepare nanocrystalline materials with appropriate structural characteristics [19–21]. In this method, melting is not

*Corresponding author. Tel.: +98 3114456551; fax: +98 3312291008.
E-mail address: bahman_nasiri@hotmail.com (B. Nasiri-Tabrizi).

0272-8842/$ - see front matter © 2013 Elsevier Ltd and Techna Group S.r.l. All rights reserved.
http://dx.doi.org/10.1016/j.ceramint.2012.12.093

essential and the products have nanostructural characteristics [22]. Thus, when the mass production of n-HAp is required, mechanochemical method can be served. In this process, milling media are often selected based on their high hardness, e.g. WC or SiC, or their chemical inertness, e.g. hardened stainless steel [23]. The use of polymeric milling media has been proposed not only to annihilate contamination problem, but also to achieve the modified morphologies with high biomedical performance [24,25]. It has been reported that the size and number of balls had no significant effect on the synthesizing time and grain size of calcium phosphates, while decreasing the rotation speed or ball to powder weight ratio increased synthesizing time and the grain size of bioceramic [26]. These results suggest that the mechanochemical synthesis of calcium phosphates is affected by processing parameters. Therefore, evaluation of milling parameters to synthesize a pure product with appropriate structural as well as morphological features is necessary.

Table 1
Details of milling conditions and composition of powder mixtures.

Sample	Composition	Milling atmosphere	Milling time (h)
HA1	100 wt% ($CaHPO_4+Ca(OH)_2$)	Air	40
HA2	100 wt% ($CaHPO_4+Ca(OH)_2$)	Argon	40
HA3	100 wt% ($CaHPO_4+Ca(OH)_2$)	Air	80
HA4	100 wt% ($CaHPO_4+Ca(OH)_2$)	Argon	80
HA5	100 wt% ($CaCO_3+CaHPO_4$)	Air	40
HA6	100 wt% ($CaCO_3+CaHPO_4$)	Argon	40
HA7	100 wt% ($CaCO_3+CaHPO_4$)	Air	80
HA8	100 wt% ($CaCO_3+CaHPO_4$)	Argon	80
HA9[a]	n-HAp	–	–

[a]Heat treated sample at 800 °C for 1 h.

Although, a variety of nanocrystalline calcium phosphates with various structural and morphological characteristics were known, but to author's knowledge, there are a few papers about the mechanosynthesis of calcium phosphates under inert gas atmosphere [27]. Mechanochemical synthesis of nano-size single crystal HAp under air atmosphere has been investigated by our group recently [24]. In this study, the influence of milling parameters (time and atmosphere) on the formation of n-HAp using different raw materials was studied. Furthermore, the milled sample was heat treated at 800 °C for 1 h to produce n-HAp with high degree of crystallinity. The phase purity of the HAp nanopowders, average crystallite size, lattice strain, volume fraction of grain boundary, fraction of crystalline phase (crystallinity) and morphological features of experimental outcomes were also determined.

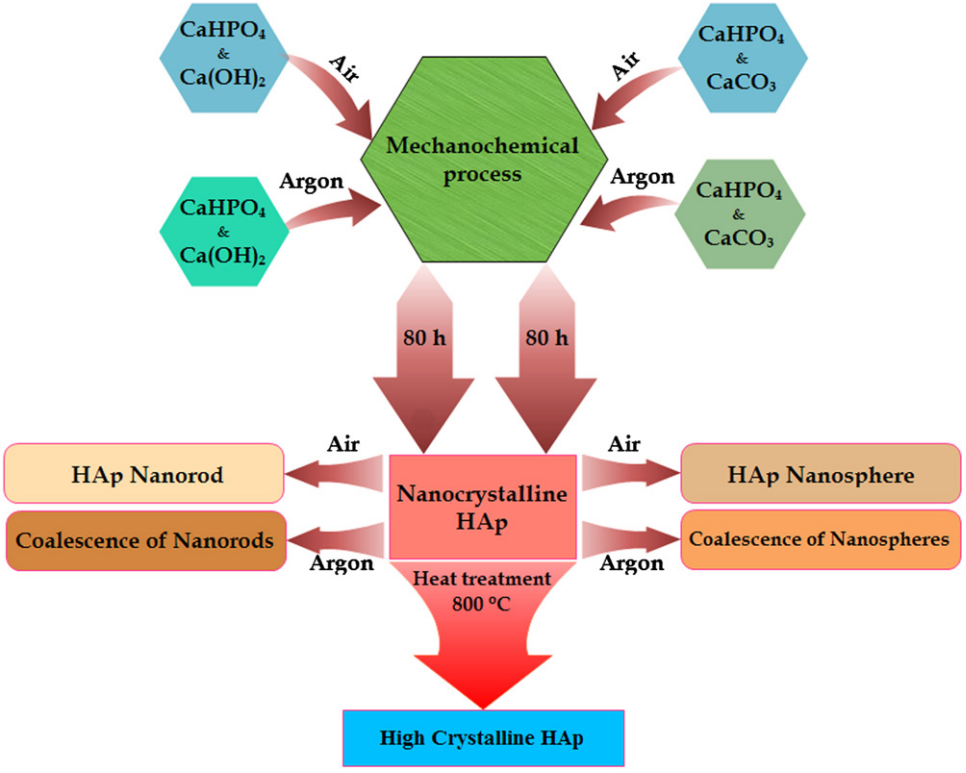

Fig. 1. The solid-sate process for preparation of n-HAp.

2. Materials and methods

2.1. Preparation of n-HAp powders

Starting materials including calcium hydroxide ($Ca(OH)_2$, Fluka), anhydrous dicalcium phosphate ($CaHPO_4$, Merck) and calcium carbonate ($CaCO_3$, Merck) with given stoichiometric proportionality within the reagents were milled using a high energy planetary ball mill under air or in a purified argon (99.998 vol%) atmosphere. Details of milling conditions and composition of powder mixtures are given in Table 1. Mechanical activation was performed in polyamide-6 vials (volume of 125 ml) using Zirconia balls (20 mm in diameter) for 15, 40 and 80 h. The weight ratio of ball-to-powder and rotational speed were 20:1 and 600 rpm, respectively. To control temperature and prevent excessive heat, the millings were completed in 45 min milling steps with 15 min interval pauses. In order to investigate the effect of chemical composition of raw materials on the mechanosynthesis and purity of final products, two distinct chemical reactions were utilized as follows:

$$6CaHPO_4 + 4Ca(OH)_2 \rightarrow Ca_{10}(PO_4)_6(OH)_2 + 6H_2O \quad (1)$$

$$4CaCO_3 + 6CaHPO_4 \rightarrow Ca_{10}(PO_4)_6(OH)_2 + 4CO_2 + 2H_2O \quad (2)$$

Subsequently, the mechanically activated powder was filled in a quartz boat, and then annealed for 1 h under atmospheric pressure at 800 °C. The heating rate from room temperature up to the desired temperature was fixed at 10 °C min^{-1}. The whole solid-sate process for preparation of n-HAp is presented in Fig. 1.

2.2. Characterization of n-HAp powders

Phase analysis of products was carried out by X-ray diffraction (Philips X-ray diffractometer (XRD), *Cu-*K_α radiation, 40 kV and 30 mA). "PANalytical X'Pert HighScore" software was used for the analysis of the diffraction patterns. The patterns were compared to standards compiled by the Joint Committee on Powder Diffraction and Standards (JCPDS), which involved card #24-0033 for HAp, #09-0080 for $CaHPO_4$, #01-0837 for $CaCO_3$ and #04-0733 for $Ca(OH)_2$. Crystallite size and lattice strain of the samples were determined using the XRD data according to the following equations [19,28]:

$$D = \frac{K\lambda}{(b_{obs} - b_{std})(b\cos\theta)} \quad (I)$$

$$E^2 = \frac{(b_{obs}^2 - b_{std}^2)}{(4\tan\theta)^2} \quad (II)$$

where b (in radians), K, λ, D, E and θ are the structural broadening, shape coefficient (value between 0.9 and 1.0), the wavelength of the X-ray used (0.154056 nm), crystallite size, lattice strain and the Bragg angle (deg.), respectively.

If we assume that a crystallite is a sphere of diameter D surrounded by a shell of grain boundary with thickness t, the volume fraction of grain boundary, f, is approximately [29]:

$$f = 1 - \left[\frac{D}{(D+t)}\right]^3 \quad (III)$$

Values of f were calculated from this equation by substituting the experimental crystallite size obtained by XRD with D under the assumption of $t = 1$ nm.

Moreover, the relation between lattice spacing (d) and lattice parameters (a, b and c) of the n-HAp was shown as [30].

$$\frac{1}{d^2} = \frac{4}{3}\frac{h^2 + hk + k^2}{a^2} + \frac{l^2}{c^2} \quad (IV)$$

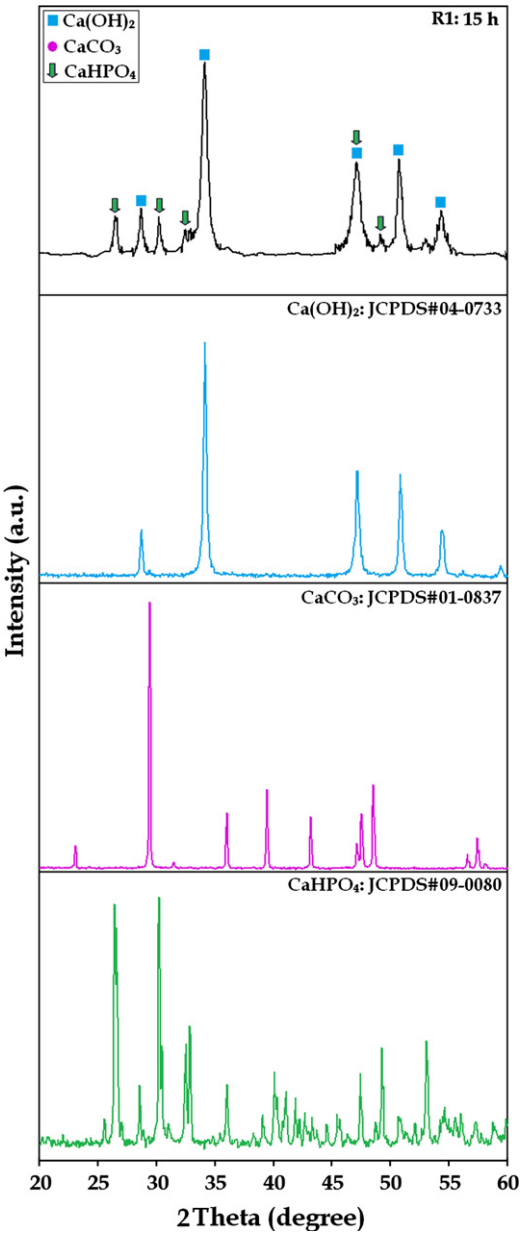

Fig. 2. XRD profile of reaction (1) after 15 h of milling compared with standard cards.

where h, k, l are the Miller indices of the reflection planes. The (002) and (300) reflections were chosen for the lattice parameters calculation. In addition, volume V of the hexagonal unit cell was determined by the following formula [31]:

$$V = 2.589a^2c \quad \text{(V)}$$

The fraction of crystalline phase (crystallinity) was determined from the XRD data using the following equation [32]:

$$B_{hkl}\sqrt[3]{X_c} = \mathrm{K} \quad \text{(VI)}$$

where X_c, K and B are the fraction of crystalline phase, a constant found equal to 0.24 and FWHM (deg.) of selected reflection peaks, respectively. It should be mentioned that the structural features of n-HAp powders were repeated two times for two groups of peaks; one group was (002), (211) and (300), and another was (222), (004) and (213) miller's planes family. The average of these two measurements was presented as mean fraction of crystalline phase, crystallite size and lattice strain. Fourier transform infrared (FT-IR) spectra were recorded on a JASCO—(FT/IR-6300, Japan) spectrometer in the range of 4000–400 cm^{-1} using KBr pellets. Energy dispersive X-ray spectroscopy (EDX) which was coupled with SEM (SERON AIS-2100) was utilized for semi-quantitative examination of the samples (voltage used for EDX equal to 20 kV). Field emission scanning electron microscope (FE-SEM Hitachi S1831) was served to observe the morphology of heat treated sample that operated at the acceleration voltage of 15 kV. Besides, the size and morphology of fine powders and agglomerates were observed on a transmission electron microscope (ZEISS, Germany) that operated at the acceleration voltage of 80 kV. TEM samples were prepared using ultrasonic devices (Misonix, S3000).

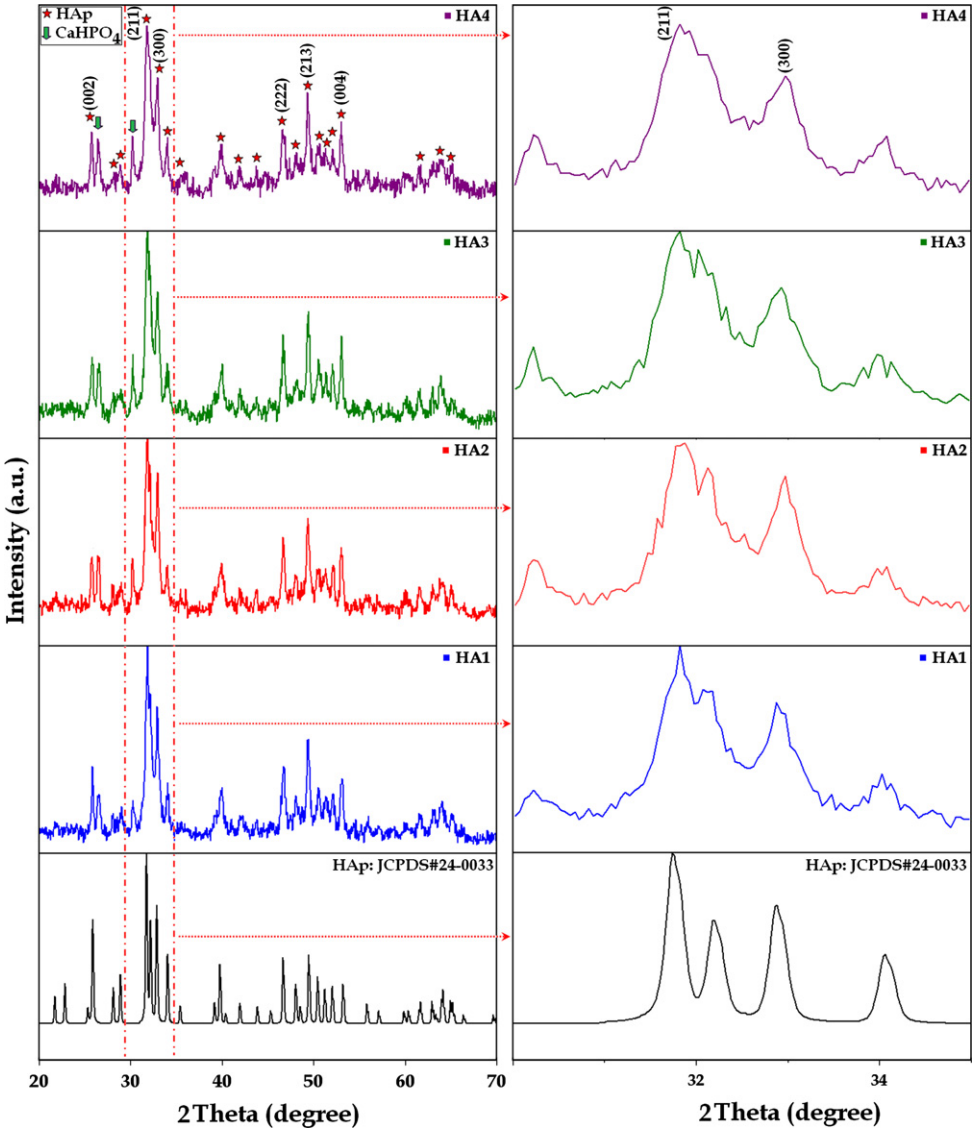

Fig. 3. XRD patterns of reaction (1) after 40 and 80 h of milling under air and argon atmospheres.

3. Results and discussion

3.1. Phase determination

Fig. 2 presents XRD profile of reaction (1) after 15 h of milling. This figure shows that there is no trace of HAp after 15 h of milling due to the lack of sufficient time for mechanical activation. In fact, the particle size reduction begins after 15 h of milling while no reaction takes place within powders. Fig. 3 shows the XRD patterns of reaction (1) after 40 and 80 h of milling under air and argon atmospheres. As can be seen in this figure, the main product was HAp after 40 and 80 h under both milling atmospheres. In addition, the extra peaks related to $CaHPO_4$ can also be seen in the samples. It has been reported that the presence of $CaHPO_4$ as an extra phase could be a trace of the original product of the original reaction used to produce n-HAp [22]. This suggests that the synthesized HAp had the Ca/P ratio lower than stoichiometry value as a result of $CaHPO_4$ formation after 40 and 80 h of milling. Fig. 4 displays XRD profile of reaction (2) after 15 h of milling. In this reaction, $CaHPO_4$ and $CaCO_3$ were used as raw materials but after 15 h of milling, similar to previous reaction, HAp was not produced. Moreover, sharp characteristic peaks of $Ca(OH)_2$ as an intermediate phase appeared in XRD pattern. It seems that the decomposition of $CaCO_3$ occurred after 15 h of milling which resulted in the formation of $Ca(OH)_2$ through the following reactions:

$$xCaCO_3 \rightarrow xCaO + xCO_2 \quad (3)$$

$$xCaO \rightarrow xH_2O + xCa(OH)_2 \quad (4)$$

When the mechanical activation time was extended to 40 h, all the peaks corresponding to $CaHPO_4$, $CaCO_3$ and $Ca(OH)_2$ had vanished and only those belonging to HAp was detectable (reaction (5)). Further increase in milling time up to 80 h resulted in the formation of low crystalline HAp as evidenced by further broadening of the principal diffraction peaks (Fig. 5).

$$6CaHPO_4 + xCa(OH)_2 + (4-x)CaCO_3 \rightarrow Ca_{10}(PO_4)_6(OH)_2 + (2+x)H_2O + (4-x)CO_2 \quad (5)$$

This result indicates that the phase purity of mechanosynthesized HAp affected by chemical composition of raw materials. Comparison of the obtained results revealed that the nature of final phases was not influenced by inert gas atmosphere as a result a same phase structure was obtained under both milling atmospheres. According to XRD patterns, the use of the reaction (2) is preferred to reaction (1) in order to produce HAp with higher phase purity.

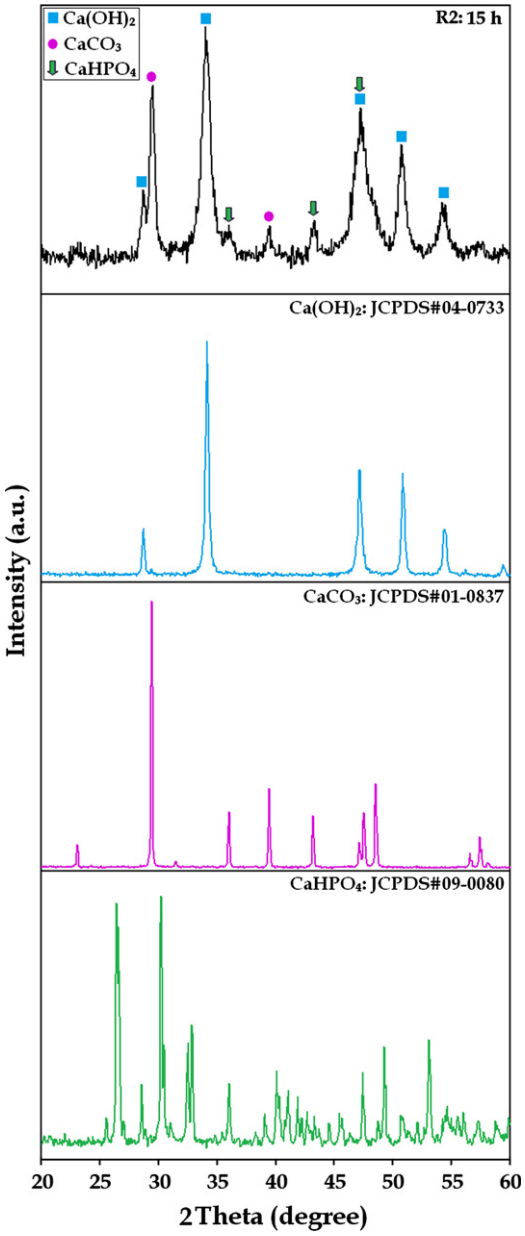

Fig. 4. XRD profile of reaction (2) after 15 h of milling compared with standard cards.

3.2. Crystallite size, lattice strain and volume fraction of grain boundary

Fig. 6 shows the effect of milling time under both milling atmospheres on the average crystallite size, volume fraction of grain boundaries and lattice strain of HAp. Based on the calculated data, the average crystallite size of HAp out of reaction (1) under both milling atmospheres was around 37 and 32 nm after 40 and 80 h of milling, respectively (Fig. 6a). Also, the volume fraction of grain boundary of n-HAp was about 7.689% after 40 h and 8.818% after 80 h of milling (Fig. 6b). The evaluation of lattice strain demonstrated that the lattice strain of the samples was about 0.306% after 40 h and 0.356% after 80 h of milling under air atmosphere (Fig. 6c). These values were about 0.298% after 40 h and

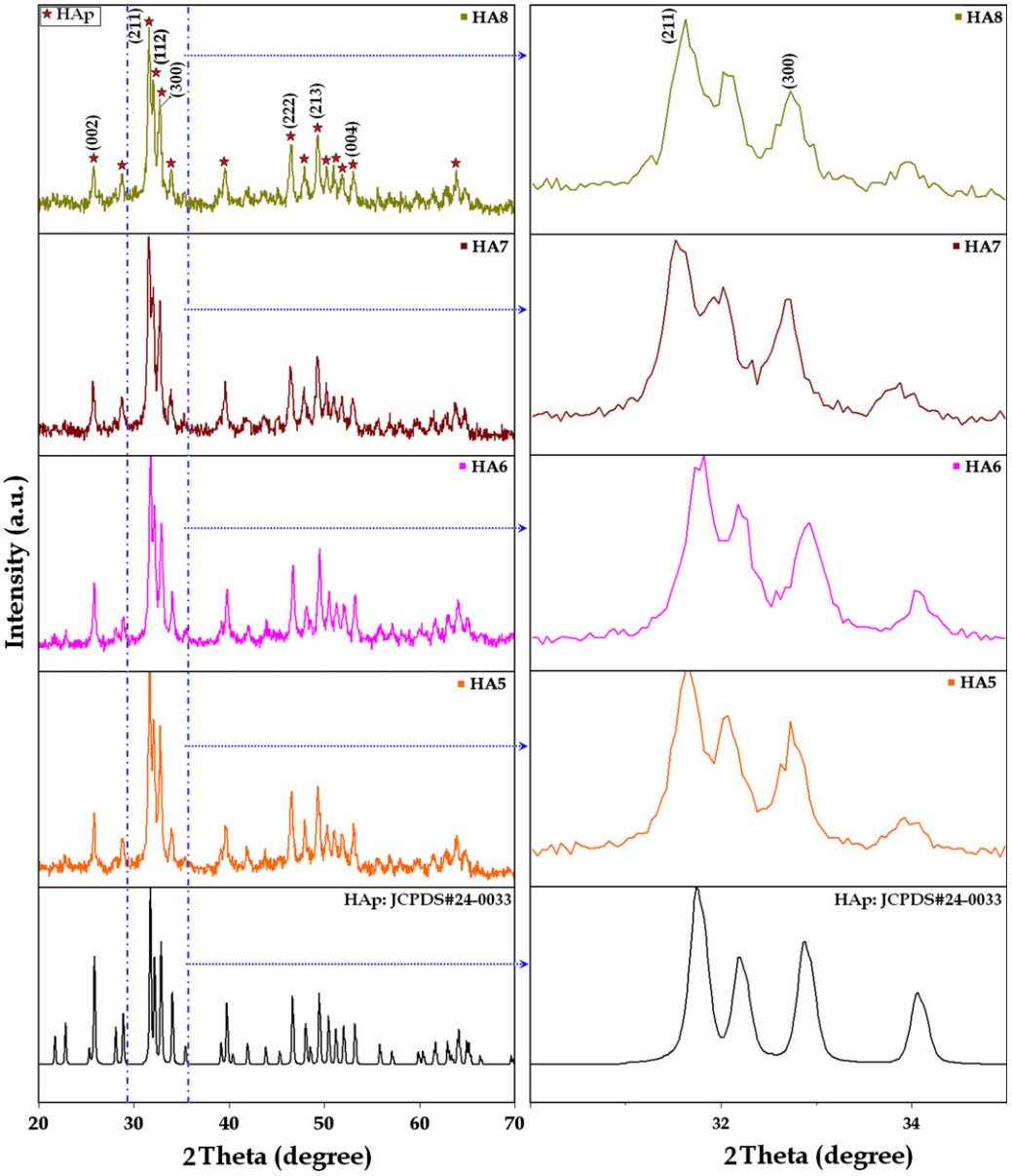

Fig. 5. XRD patterns of reaction (2) after 40 and 80 h of milling under air and argon atmospheres.

0.371% after 80 h of milling under argon atmosphere. On the other hand, the average crystallite size of HAp out of reaction (2) under air atmosphere was around 33 and 27 nm after 40 and 80 h of milling, respectively (Fig. 6d). These values were about 40 nm after 40 h and 34 nm after 80 h of milling under argon atmosphere. The volume fraction of grain boundary of n-HAp under air atmosphere was about 8.567 and 10.336% after 40 and 80 h of milling, respectively (Fig. 6e). For the milled samples under argon atmosphere, these values were about 7.140% after 40 h and 8.329% after 80 h of milling. The determined amounts of lattice strain indicated that by increasing milling time to 80 h, the average lattice strain increased under both milling atmospheres (Fig. 6f). The lattice strain reached 0.409 and 0.304% after 80 h of milling under air and argon atmospheres, respectively. It should be noted that the decrease rate of crystallite size in reaction (2) is higher than that in reaction (1) under both milling atmospheres. However, results revealed that increasing the milling time causes decreasing the crystallite size and increasing the lattice strain.

3.3. Fraction of crystalline phase (crystallinity)

For the evaluation of the fraction of crystalline phase, peak broadening is an important parameter. In this paper, full width at half maximum (FWHM) of specified peaks was utilized to determine the fraction of crystalline phase. Fig. 7a and c shows the FWHM values at different Bragg angles for all the samples where the anisotropy is most pronounced. Examination of the FWHM values for all the specimens revealed the occurrence of anisotropic line broadening. In general, the anisotropic line broadening

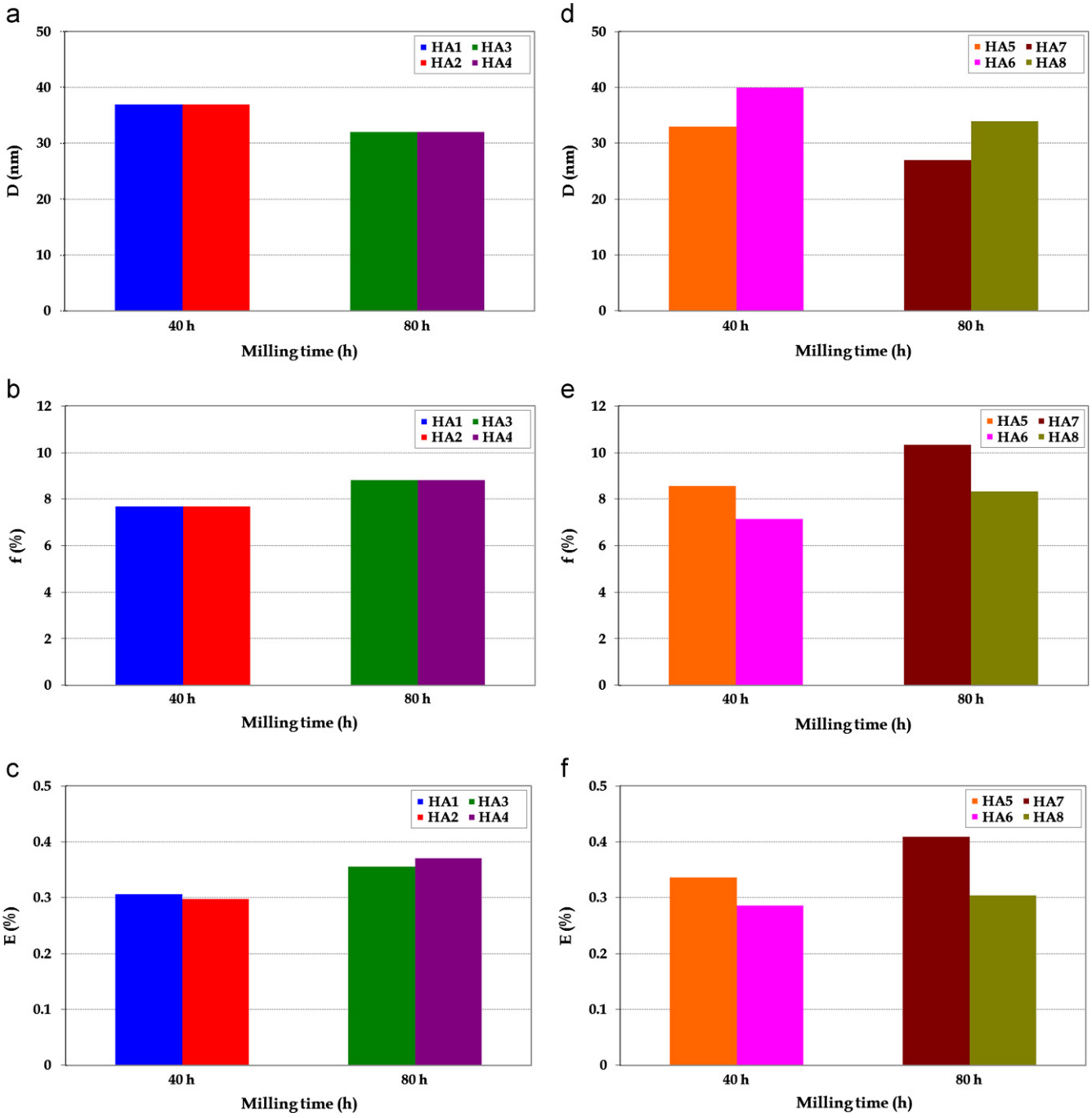

Fig. 6. The average crystallite size, volume fraction of grain boundaries and lattice strain of HAp as a function of milling time under both milling atmospheres; (a–c) reaction (1) and (d–f) reaction (2).

may be ascribed to the three factors: the presence of stacking faults, the presence of dislocations and non-equivalence of the grain sizes along different crystallographic directions [33]. In our case, it seems that this phenomenon is due to the grain size anisotropy. According to Fig. 7b and d, by increasing milling time to 80 h, the fraction of crystalline phase decreased for both reactions under air and argon atmospheres. In general, control of the crystallinity of HAp is necessary for its biological applications. Since high crystallinity of HAp shows little or no activity toward bioresorption and is insoluble in physiological environment [34], the HA1, HA2, and HA6 samples are well preferred for dental applications. On the other side, the HAp powders with lower degree of crystallinity including HA3, HA4, HA5, HA7 and HA8 can be used to promote osseointegration or as a coating to promote bone in growth in to prosthetic implants [35].

3.4. Lattice parameters

To confirm the formation of HAp, the lattice parameters of the samples were calculated, as shown in Fig. 8. As can

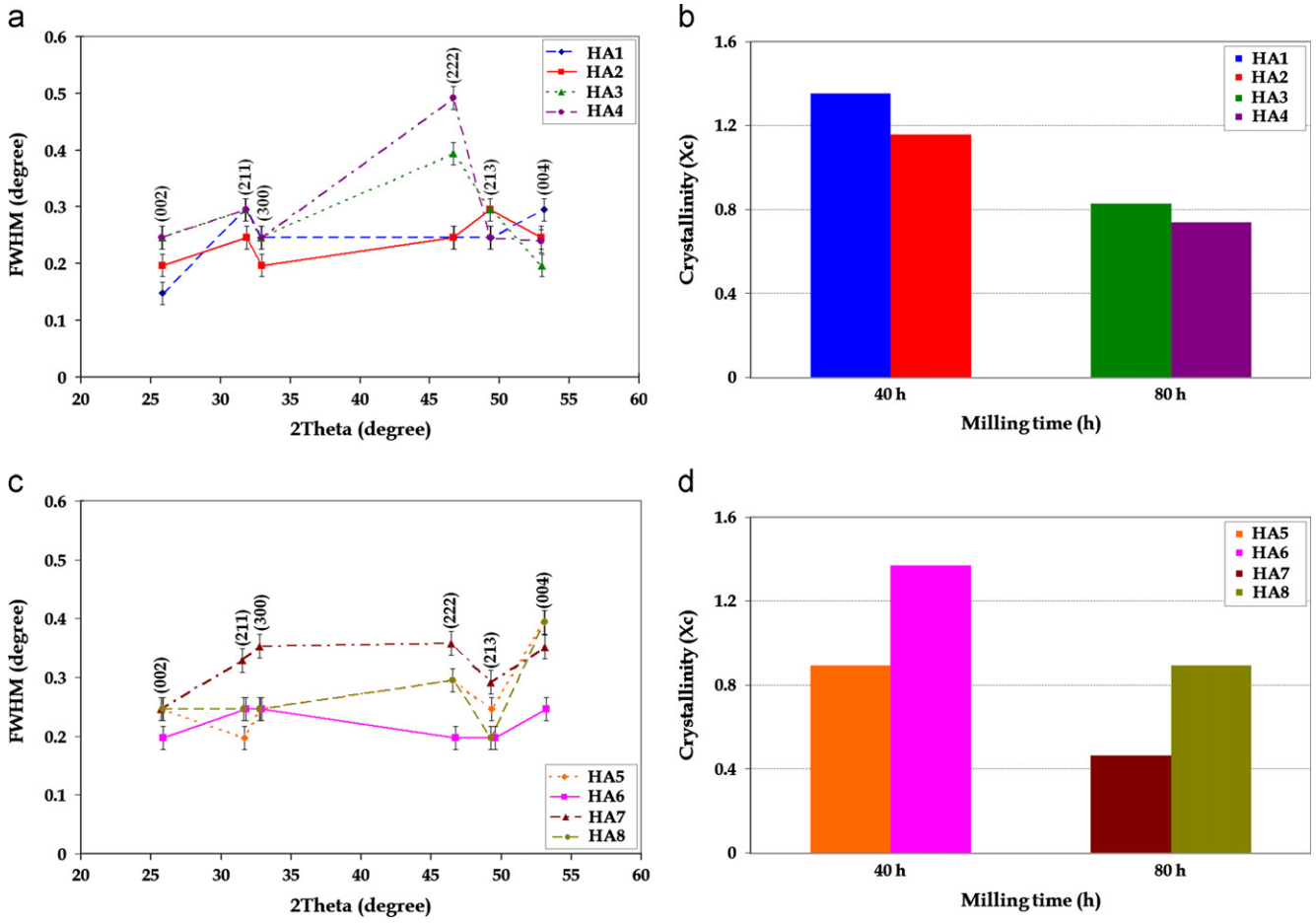

Fig. 7. (a,c) The FWHM values at different Bragg angles for the milled samples and (b,d) the fraction of crystalline phase as a function of milling times under air and argon atmospheres.

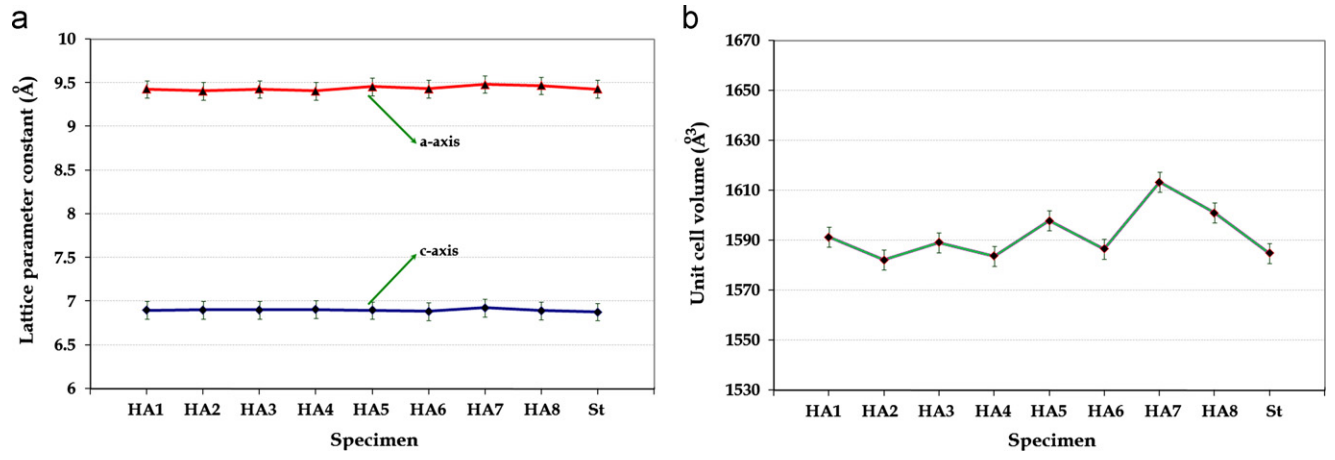

Fig. 8. (a) Change in the lattice constants and (b) their unit cell volume for HAp as a function of production conditions.

be seen in Fig. 8, the *a*-axis and *c*-axis values were similar to the standard HAp (#24-0033: $a=9.432$ Å and $c=6.881$ Å). The determined amounts of unit cell volume of HAp showed that the experimental outcomes out of reaction (1) were not accompanied by a remarkable change in the unit cell volume under both milling atmospheres. Conversely, the obtained powders out of reaction (2) showed remarkable changes in the unit cell volume, particularly in HA7 and HA8 samples. These changes in the unit cell volume can probably be attributed to the lattice distortion of HAp

during the mechanochemical process. The results showed that the lattice parameters of mechanosynthesized HAp affected by chemical composition of raw materials and milling atmospheres.

3.5. TEM observations

The morphological characteristics of the n-HAp out of reaction (1) after 80 h milling under both milling atmospheres are shown in Fig. 9. The TEM observations showed that the HAp particles had rod-like morphology with an average length of about 20 and 25 nm under air and argon atmospheres, respectively. Although, in outcomes from reaction (1), there are some particles with ellipse-like morphology, it is because of the axis orientation of nanorods with respect to the image plane. In fact, if the rod axis is perpendicular or oblique to the image plane, the rod may be seen as a full circle or ellipse shape, subsequently. It has been found that the n-HAp with ellipse- or rod-like morphology inhibit the proliferation of malignant melanoma cells [36]. Therefore, these nanostructures may be helpful to remedy cancer. Furthermore, since the synthetic HAp nanorods have an excellent sinterability [24], using this structure is an effective route to obtain dense bioceramics with high mechanical properties. As a result, the gained HAp nanorods may be utilized as strength-enhancing additives for the preparation of the bionanocomposites with improved mechanical properties.

Fig. 10 shows the TEM images of n-HAp out of reaction (2) after 80 h milling under both milling atmospheres. According to this figure, the HAp particles had spheroidal morphology with an average size of about 23 and 25 nm under air and argon atmospheres, respectively. It has been found that spherical particles are better than other irregular shapes due to the well space fillings and the low percentage of voids in the final product [24]. Besides, granules with a smooth spherical geometry are useful in growth and attachment of bone tissue that improve osseointegration.

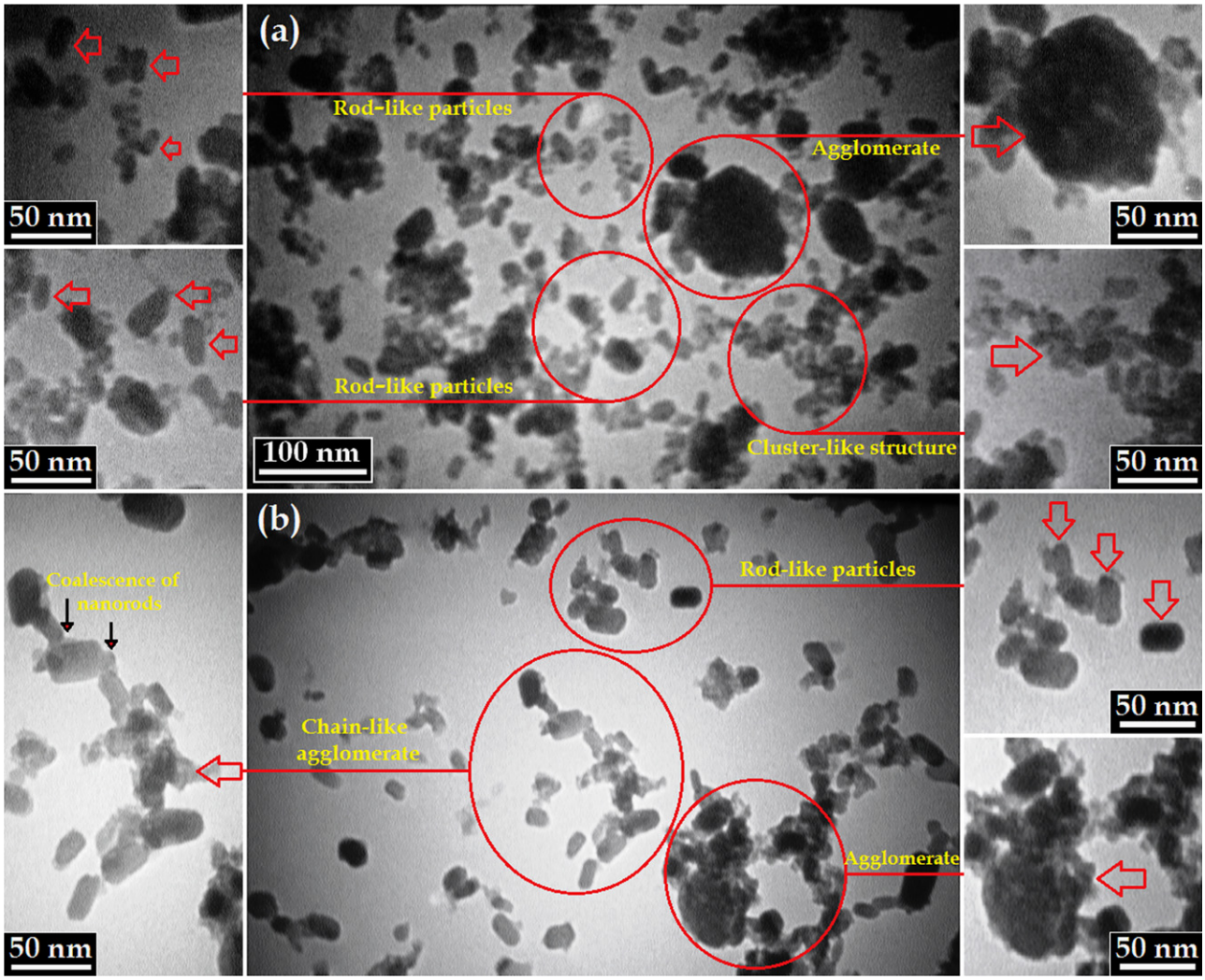

Fig. 9. TEM images of n-HAp powders produced through reaction (1) after 80 h milling under (a) air and (b) argon atmospheres.

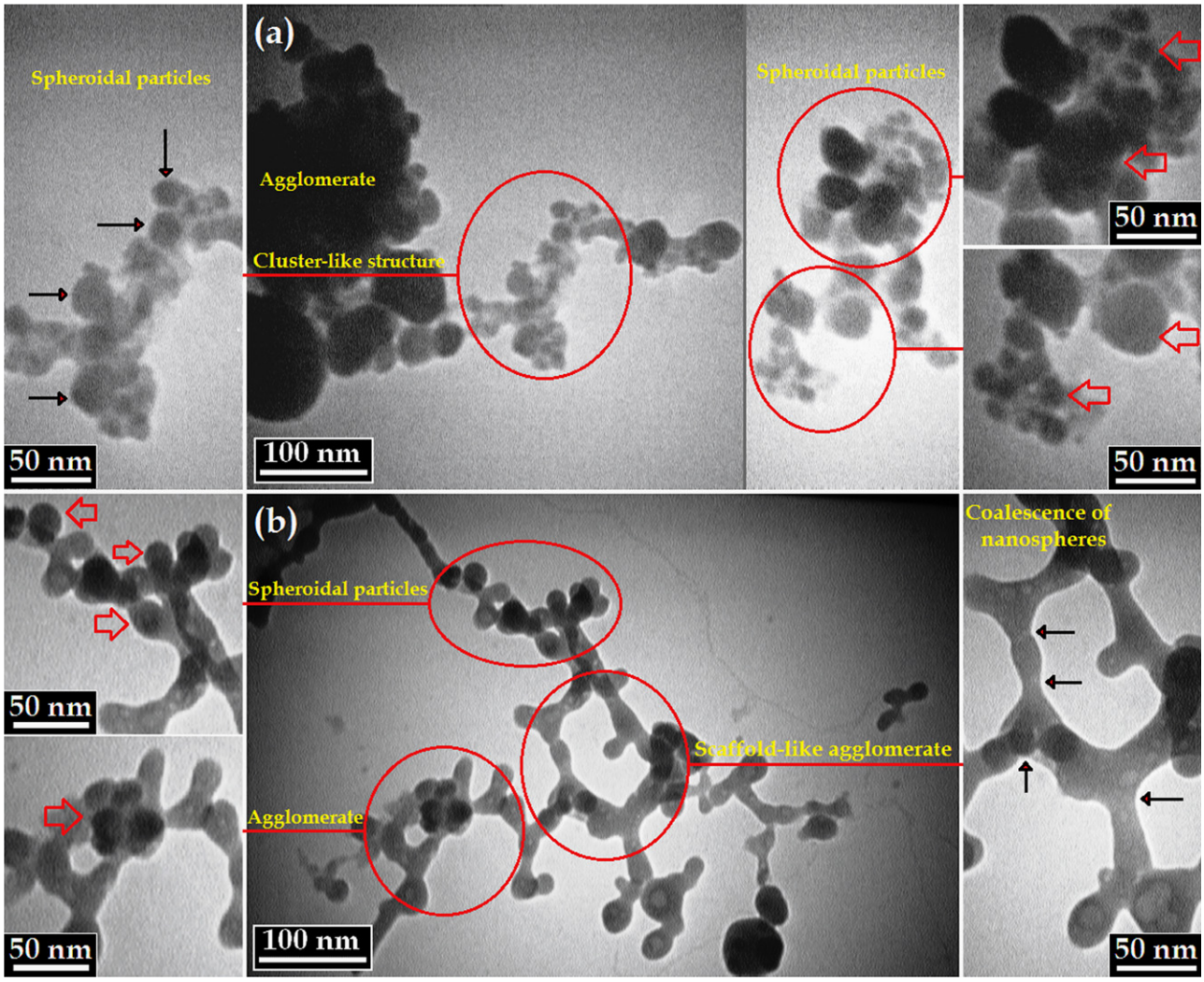

Fig. 10. TEM images of n-HAp powders produced through reaction (2) after 80 h milling under (a) air and (b) argon atmospheres.

In addition to presented results, it is obvious that the milled samples had a high agglomeration tendency. According to literature [19], when two adjacent primary particles collide, the coalescence may take place on the premise that these two particles share a common crystallographic orientation. So, two primary particles attach to each other and combine into a secondary one. Since the sizes of the secondary particles are still very small, it is reasonable that they will continue to collide and coalesce which may ultimately lead to the agglomeration. As shown in Figs. 9 and 10b, the coalescence of nanorods and nanospheres led to the formation of agglomerates after 80 h of milling under argon atmosphere. It has been found that the deformation of the smaller particle and convection processes controlled the coalescence of liquid nanoparticles. On the other hand, diffusion processes dominated the coalescence processes of near solid-like particles [37]. Thus, in present study, it seems that the coalescence of nanorods and nanospheres occurred under argon atmosphere because of diffusion process. Recalling from the above results, it can be concluded that the mechanochemical method is an appropriate dry process to synthesize n-HAp with different structural as well as morphological features which can be considered for specific targets.

3.6. Heat treatment

Fig. 11 shows the XRD profile and FT-IR spectrum of n-HAp after thermal treatment at 800 °C. The XRD pattern of annealed sample confirmed the formation of high crystalline HAp with appropriate phase purity (Fig. 11a). As can be seen in this figure, the intensity of the peaks of the main reflections increased after thermal treatment. This result confirms the growth of the crystallinity after thermal treatment at 800 °C. The evaluation of the structural features indicated that the average crystallite size and the volume fraction of grain boundary were around 43 nm and 6.664%, respectively. Furthermore, the fraction of crystalline phase enhanced after thermal treatment at 800 °C. The obtained result suggests that the fraction of crystalline phase was higher for the annealed sample compared to the mechanosynthesized specimens. The FT-IR analysis was carried out to get authenticated information about the functional group and to confirm the production

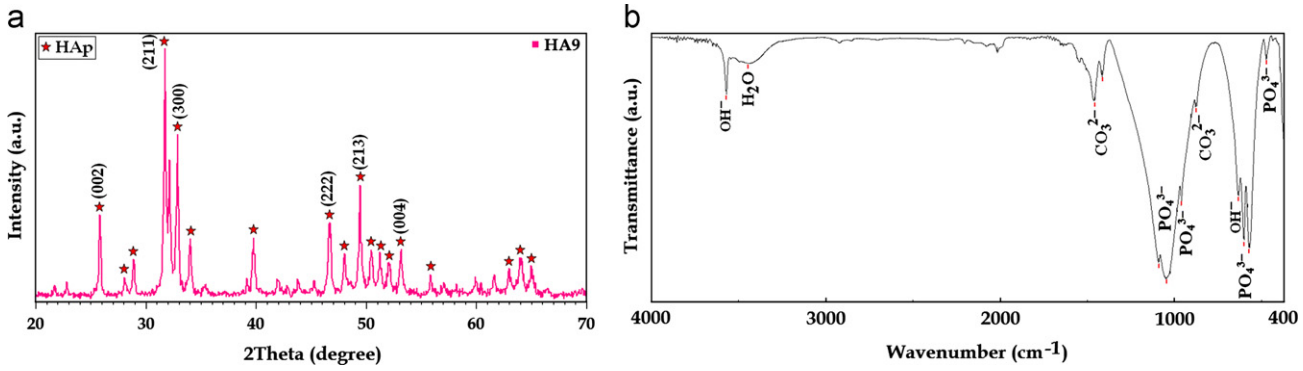

Fig. 11. XRD profile and FT-IR spectrum of n-HAp after thermal treatment at 800 °C for 1 h.

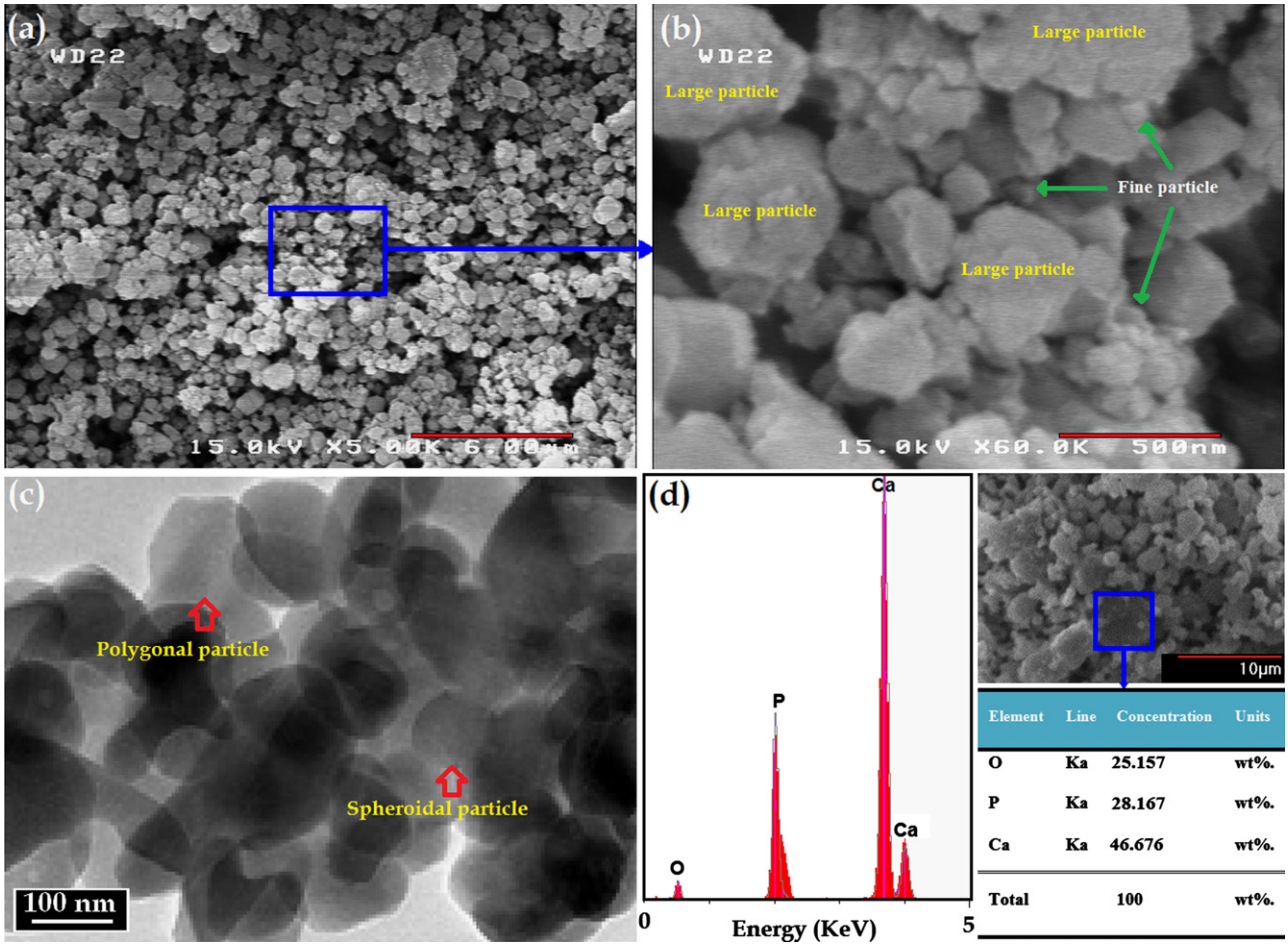

Fig. 12. (a,b) FE-SEM observations, (c) TEM image and (d) EDX spectra of n-HAp after thermal treatment at 800 °C.

of HAp with no chemically stable contaminants. In Fig. 11b, two bands corresponding to the vibration of the adsorbed water in the apatite structure were detected [19,38]. A doublet appears at 1414 and 1457 cm^{-1} corresponding to v_3 and a band at 878 cm^{-1} attributed to v_2 vibration mode of the carbonated groups which showed the n-HAp contained some CO_3^{2-} groups in PO_4^{3-} sites of apatite lattice (B-type substitution) [28,38]. It has been reported that this kind of apatite is more similar to biological apatite and could be more suitable for bone replacement materials [39]. The characteristic peaks of the phosphate group had four distinct asymmetrical stretching vibration modes, namely, v_1, v_2, v_3 and v_4. The v_1 and v_2 vibration peaks were observed at 961 and 472 cm^{-1}, respectively. The v_3 vibration peaks as a major peak of the phosphate group were detected in the region between 1090 and 1048 cm^{-1}. The band between 602 and 569 cm^{-1} showed v_4 vibration mode of phosphate group. Results indicated that the synthesized powder has a suitable chemical purity.

Fig. 12 shows the morphology, particle size distribution and EDX spectra of n-HAp after thermal treatment at

800 °C. From TEM and FE-SEM images (Fig. 12a–c), it can be seen that the product was composed of large and fine particles with spheroidal and polygonal morphologies. The average particle size of the sample was about 116 nm. Based on these observations, the mean particle size of n-HAp powders were smaller for the milled samples compared to the annealed specimen due to the large amount of strain imparted to particles during the milling process. Fig. 12d shows the EDX spectra of the n-HAp after thermal treatment at 800 °C. As expected, EDX spectra showed that the main elements of the specimen were calcium, phosphorus and oxygen. The EDX spectrum of HAp crystals exhibited a molar ratio Ca/P=1.66. These results demonstrate that the HAp crystals are closer to the standard HAp (Ca/P=1.67). According to the EDX point chemical analysis, no chemically stable contaminants were detected due to the excessive adhesion of powders to the milling media. In accordance with our previous findings [18,19,24,25,28], the polyamide-6 vial is a suitable milling media to annihilate contamination problem and to achieve modified morphologies with high biomedical performance.

4. Conclusions

The effect of milling parameters on the mechanosynthesis of n-HAp using different raw materials was investigated. Moreover, the milled powder was heat treated at 800 °C for 1 h to produce n-HAp with high degree of crystallinity. The results showed that the phase purity of mechanosynthesized HAp affected by chemical composition of raw materials, so that the use of the reaction (2) is preferred to reaction (1) in order to produce n-HAp with higher phase purity. The nature of final phases was not influenced by inert gas atmosphere as a result a same phase structure was obtained under both milling atmospheres. By increasing the milling time, the crystallite size decreased and reached a minimum after 80 h of milling. Examination of the full width at half maximum values for all the samples indicated the occurrence of anisotropic line broadening. Furthermore, the determined amounts of crystallinity revealed that the fraction of crystalline phase was lower for the mechanosynthesized samples compared to the annealed specimen. Based on TEM observations, the mean particle size of n-HAp powders was smaller for milled sample compared to the annealed specimen. After thermal treatment at 800 °C, the product was composed of spheroidal and polygonal particles with an average size of about 116 nm.

Acknowledgment

The authors are grateful to research affairs of Islamic Azad University, Najafabad Branch for supporting this research.

References

[1] P.Q. Franco, C.F.C. João, J.C. Silva, J.P. Borges, Electrospun hydroxyapatite fibers from a simple sol–gel system, Materials Letters 67 (2012) 233–236.
[2] Y. Feng, G. Haifeng, Z. Haijiao, H. Xiulan, Polymeric micelle-templated synthesis of hydroxyapatite hollow nanoparticles for a drug delivery system, Acta Biomaterialia 6 (2010) 2212–2218.
[3] O. Ichiro, Y. Toshiharu, J. Hai-Ying, I. Yoshinori, H. Hirobumi, A. Yoshikiyo, N. Masanori, O. Tetsunori, J. Kowichi, Combination of porous hydroxyapatite and cationic liposomes as a vector for BMP-2 gene therapy, Biomaterials 25 (2004) 4709–4718.
[4] S.R. Shepard, Ch. Brickman-Stone, J.L. Schrimsher, G. Koch, Discoloration of ceramic hydroxyapatite used for protein chromatography, Journal of Chromatography A 891 (2000) 93–98.
[5] P. Molle, A. Lienard, A. Gramsik, Apatite as an interesting seed to remove phosphorus from waste-water in constructed wetlands, Water Science and Technology 51 (2005) 193–203.
[6] M.N. Salimi, R.H. Bridson, L.M. Grover, G.A. Leeke, Effect of processing conditions on the formation of hydroxyapatite nanoparticles, Powder Technology 218 (2012) 109–118.
[7] E. Iyyappan, P. Wilson, Synthesis of nanoscale hydroxyapatite particles using triton X-100 as an organic modifier, Ceramics International 39 (2013) 771–777.
[8] M.H. Fathi, A. Hanifi, V. Mortazavi, Preparation and bioactivity evaluation of bone-like hydroxyapatite nanopowder, Journal of Materials Processing Technology 202 (2008) 536–542.
[9] Y.M. Sung, J.Ch. Lee, J.W. Yang, Crystallization and sintering characteristics of chemically precipitated hydroxyapatite nanopowder, Journal of Crystal Growth 262 (2004) 467–472.
[10] S.K. Saha, A. Banerjee, S. Banerjee, S. Bose, Synthesis of nanocrystalline hydroxyapatite using surfactant template systems: role of templates in controlling morphology, Materials Science and Engineering C 29 (2009) 2294–2301.
[11] A. Banerjee, A. Bandyopadhyay, S. Bose, Hydroxyapatite nanopowders: synthesis, densification and cell–materials interaction, Materials Science and Engineering C 27 (2007) 729–735.
[12] S.J. Kalita, A. Bhardwaj, H.A. Bhatt, Nanocrystalline calcium phosphate ceramics in biomedical engineering, Materials Science and Engineering C 27 (2007) 441–449.
[13] C.Y. Ooi, M. Hamdi, S. Ramesh, Properties of hydroxyapatite produced by annealing of bovine bone, Ceramics International 33 (2007) 1171–1177.
[14] D. Tadic, M. Epple, A thorough physicochemical characterisation of 14 calcium phosphate-based bone substitution materials in comparison to natural bone, Biomaterials 25 (2004) 987–994.
[15] Z. He, J. Ma, C. Wang, Constitutive modeling of the densification and the grain growth of hydroxyapatite ceramics, Biomaterials 26 (2005) 1613–1621.
[16] S.H. Rhee, Synthesis of hydroxyapatite via mechanochemical treatment, Biomaterials 23 (2002) 1147–1152.
[17] J.S. Cho, S.H. Rhee, Formation mechanism of nano-sized hydroxyapatite powders through spray pyrolysis of a calcium phosphate solution containing polyethylene glycol, Journal of the European Ceramic Society 33 (2013) 233–241.
[18] P. Honarmandi, P. Honarmandi, A. Shokuhfar, B. Nasiri-Tabrizi, R. Ebrahimi-Kahrizsangi, Milling media effects on synthesis, morphology and structural characteristics of single crystal hydroxyapatite nanoparticles, Advances in Applied Ceramics 109 (2010) 117–122.
[19] A. Fahami, B. Nasiri-Tabrizi, R. Ebrahimi-Kahrizsangi, Synthesis of calcium phosphate-based composite nanopowders by mechanochemical process and subsequent thermal treatment, Ceramics International 38 (2012) 6729–6738.
[20] P.F. Xiao, M.O. Lai, L. Lu, Electrochemical properties of nanocrystalline TiO_2 synthesized via mechanochemical reaction, Electrochimica Acta 76 (2012) 185–191.

[21] J. Huot, D.B. Ravnsbæk, J. Zhang, F. Cuevas, M. Latroche, T.R. Jensen, Mechanochemical synthesis of hydrogen storage materials, Progress in Materials Science 58 (2013) 30–75.
[22] C.C. Silva, A.G. Pinheiro, M.A.R. Miranda, J.C. Goes, A.S.B. Sombra, Structural properties of hydroxyapatite obtained by mechanosynthesis, Solid State Sciences 5 (2003) 553–558.
[23] C. Suryanarayana, Mechanical alloying and milling, Progress in Materials Science 46 (2001) 1–184.
[24] B. Nasiri-Tabrizi, P. Honarmandi, R. Ebrahimi-Kahrizsangi, P. Honarmandi, Synthesis of nanosize single-crystal hydroxyapatite via mechanochemical method, Materials Letters 63 (2009) 543–546.
[25] R. Ebrahimi-Kahrizsangi, B. Nasiri-Tabrizi, A. Chami, Synthesis and characterization of fluorapatite–titania (FAp–TiO_2) nanocomposite via mechanochemical process, Solid State Sciences 12 (2010) 1645–1651.
[26] E. Mohammadi Zahrani, M.H. Fathi, The effect of high-energy ball milling parameters on the preparation and characterization of fluorapatite nanocrystalline powder, Ceramics International 35 (2009) 2311–2323.
[27] T. Nakano, A. Tokumura, Y. Umakoshi, Variation in crystallinity of hydroxyapatite and the related calcium phosphates by mechanical grinding and subsequent heat treatment, Metallurgical and Materials Transactions A 33 (2002) 521–528.
[28] B. Nasiri-Tabrizi, A. Fahami, Synthesis and characterization of fluorapatite–zirconia composite nanopowders, Ceramics International, http://dx.doi.org/10.1016/j.ceramint.2012.11.016, in press.
[29] F. Sun, F.H.S. Froes, Synthesis and characterization of mechanical-alloyed Ti_xMg alloys, Journal of Alloys and Compounds 340 (2002) 220–225.
[30] J. Qian, Y. Kang, W. Zhang, Z. Li, Fabrication, chemical composition change and phase evolution of biomorphic hydroxyapatite, Journal of Materials Science: Materials in Medicine 19 (2008) 3373–3383.
[31] Z. Evis, Reactions in hydroxylapatite–zirconia composites, Ceramics International 33 (2007) 987–991.
[32] E. Landi, A. Tampieri, G. Celotti, S. Sprio, Densification behavior and mechanisms of synthetic hydroxyapatites, Journal of the European Ceramic Society 20 (2000) 2377–2387.
[33] I.N. Leontyev, V.E. Guterman, E.B. Pakhomova, P.E. Timoshenko, A.V. Guterman, I.N. Zakharchenko, G.P. Petin, B. Dkhil, XRD and electrochemical investigation of particle size effects in platinum–cobalt cathode electrocatalysts for oxygen reduction, Journal of Alloys and Compounds 500 (2010) 241–246.
[34] M.M. Seckler, M. Danese, S. Derenzo, J.V. Valarelli, M. Giulietti, R. Rodriguez-Clemente, Influence of process conditions on hydroxyapatite crystallinity obtained by direct crystallization, Journal of Materials Research 2 (1999) 59–62.
[35] K.P. Sanosh, M.C. Chu, A. Balakrishnan, Y.J. Lee, T.N. Kim, S.J. Cho, Synthesis of nano hydroxyapatite powder that simulate teeth particle morphology and composition, Current Applied Physics 9 (2009) 1459–1462.
[36] B. Li, B. Guo, H. Fan, X. Zhang, Preparation of nano-hydroxyapatite particles with different morphology and their response to highly malignant melanoma cells in vitro, Applied Surface Science 255 (2008) 357–360.
[37] T. Hawa, M.R. Zachariah, Coalescence kinetics of unequal sized nanoparticles, Journal of Aerosol Science 37 (2006) 1–15.
[38] G. Gonzalez, A. Sagarzazu, R. Villalba, Mechanochemical transformation of mixtures of $Ca(OH)_2$ and $(NH_4)_2HPO_4$ or P_2O_5, Materials Research Bulletin 41 (2006) 1902–1916.
[39] M.H. Fathi, E. Mohammadi Zahrani, Mechanical alloying synthesis and bioactivity evaluation of nanocrystalline fluoridated hydroxyapatite, Journal of Crystal Growth 311 (2009) 1392–1403.